Chin.J.Geochem.(2012)31:376–389
DOI: 10.1007/s11631-012-0588-9

Geology and geochemistry of the granitic rocks and associated dykes, East Gabal Nuqra, South Eastern Desert, Egypt

Ibrahim H. Ibrahim* and Mostafa E. Darwish
Nuclear Material Authority, 530 P.O. El Maadi, Cairo, Egypt
** Corresponding author, E-mail: Ibrahim170@yahoo.com*

Received March 11, 2011; accepted April 20, 2011

Abstract A crescent-shape granitic stock and associated dykes is located to the East Gabal Nuqra at the extreme western part of Wadi Natash, South Eastern Desert, Egypt. The examined granites are classified as alkali-feldspar granites and mainly consist of quartz, potash feldspars, plagioclases, and aegirine-augite. Xenotime, zircon, apatite and allanite are accessories representing the source of Y, U, Th and REEs in these rocks. These granites are characterized by high K_2O, Na_2O and Zn contents and Rb/Sr ratio. Also, they are highly enriched in high field strength elements (HFSE), especially Zr (1529×10^{-6}), Nb (100×10^{-6}), Hf (91×10^{-6}) and Y (624×10^{-6}) and light rare-earth elements (LREE, 141×10^{-6}) concentrations and strongly depleted in Ca, Mg, Sr and Eu contents. These features suggest that they are similar to A-type granites (type-2). The rhyolite dykes and granites have similar geochemical characteristics whereas the chondrite-normalized REE patterns show a LREE enriched feature with strong negative Eu-anomaly, whereas the REE pattern of trachydacites show slightly fractionated pattern with no Eu-anomaly. It is suggested that the trachydacites were generated by small degree of partial-melting deep-seated basic source. Such liquid, when subjected to fractional crystallization involving separation of plagioclases as residue, generated the alkali-feldspar granites. And further fractional crystallization gave rise to the alkali rhyolites. The igneous rock suite originated from metaluminous to alkaline trachytic magma, and was developed in a within-plate tectonic environment. The extension caused by NW-SE right-lateral shear in area led to the emplacement of the alkali-feldspar granites. The later extrusion of the alkali rhyolite and trachydacite dykes was due to cauldron subsidence.

Key words Gabal Nuqra; A-type granite; fractional crystallization; cauldron subsidence

1 Introduction

Alkaline igneous rocks are of very limited distribution in Egypt. El-Ramly et al. (1971) classified and grouped the alkaline rocks of South Eastern Desert into four main groups (Table 1). The crescent shape of the granitic intrusion and associated dykes of the East Gabal Nuqra are similar to the incomplete ring ridge of Gabal Zargat Naam defined as incomplete ring complex by El-Ramly et al. (1971). Hashad and El-Reedy (1979) used Rb/Sr isochron conventional ages together with previously published K/Ar dates in their study and suggested that three phases of alkaline igneous activity in the South Eastern Desert are as follows: a) 230±20 Ma phase, b) 140±15 Ma phase, and c) 90±20 Ma phase.

The present work aims to study the geology and petrogenesis of the granitic rocks and associated dykes located to the East Gabal Nuqra at the extreme western part of Wadi Natash, between Long. 33°44′–34°48′ E and Lat. 24°20′–24°24′ N (Fig. 1).

2 Geologic setting

The exposed igneous rock units of the study area are mainly granites (oldest), post-granitic dykes and trachybasalt flows (youngest). The granitic mass and associated dykes have crescent shapes, extending

northwestwards and being controlled by the NW-SE structural trends (Fig. 1). They have concave shape to the northeast with length exceeding 8 km and a maximum width about 4.5 km while the elevation point reaches about 200 m above Wadi level.

The main mass is mostly granitic and the country rocks are Nubian sandstones (Fig. 2a). The boundaries between these rocks are almost sharply represented by fault lines (Fig. 2b). The central part of the granitic mass is coarse to very coarse-grained granites grading eastwards and medium-grained granites westwards. They are dissected by NE-SW dextral and NW-SE sinistral faults associated with narrow altered zones (0.5−1 m in width) and characterized by moderate radioactivity. Northwards, near the tectonic contact, between the granites and the Nubian sandstone is ferruginated forming quartzitic sandstone (Fig. 2c) and the fractured filling with Mn-Fe oxides (Fig. 2d).

The eastern contact represents a thick zone of brecciation of both the granites and the Nubian sandstone and follows a north-westerly direction and dips to the north east. Against the mylonitic contact, the granites include quartz veinlets and pegmatoidal patches.

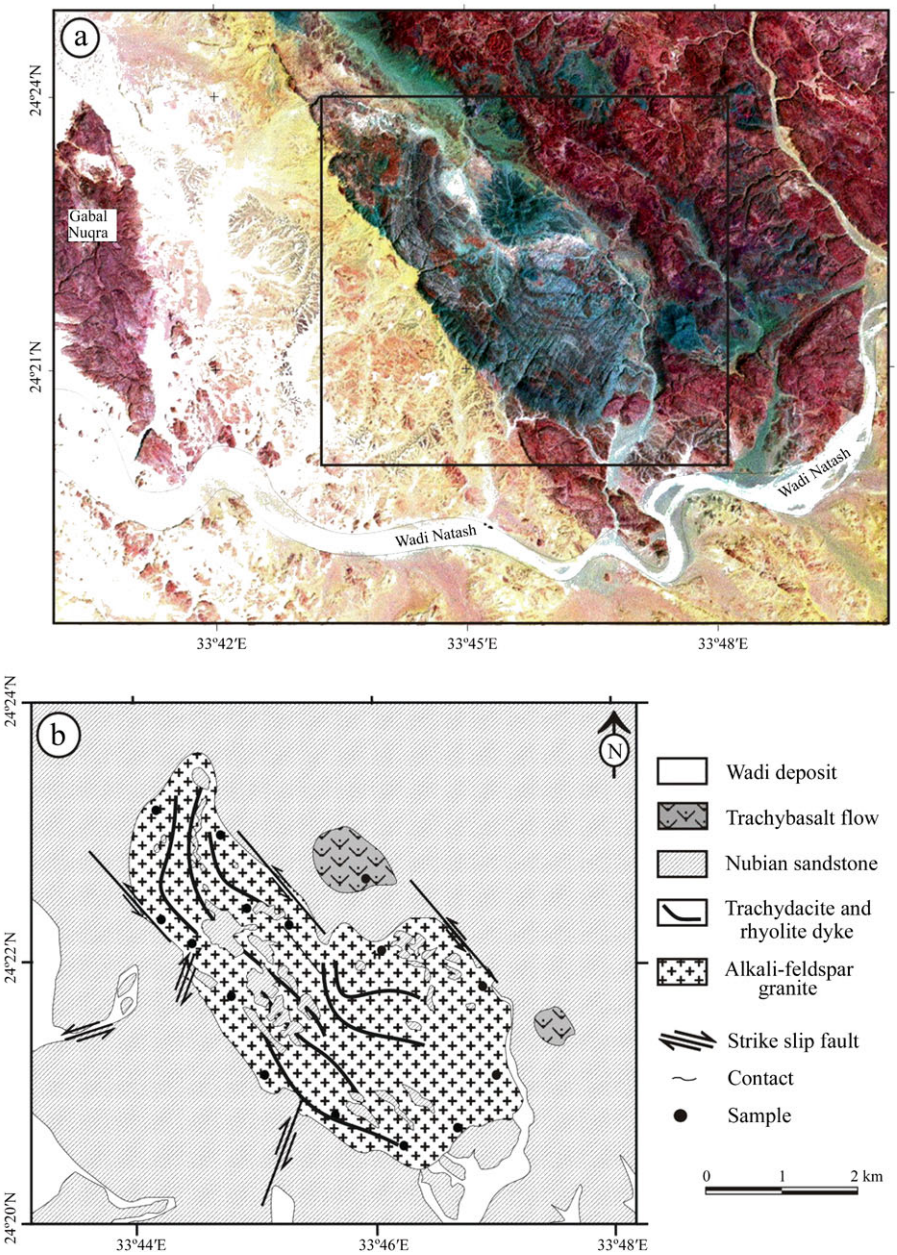

Fig. 1. Landsat TM image (5/3/2 bands) showing location of the study area to the east of Gabal Nuqra (a), geological map of the East Gabal Nuqra (b).

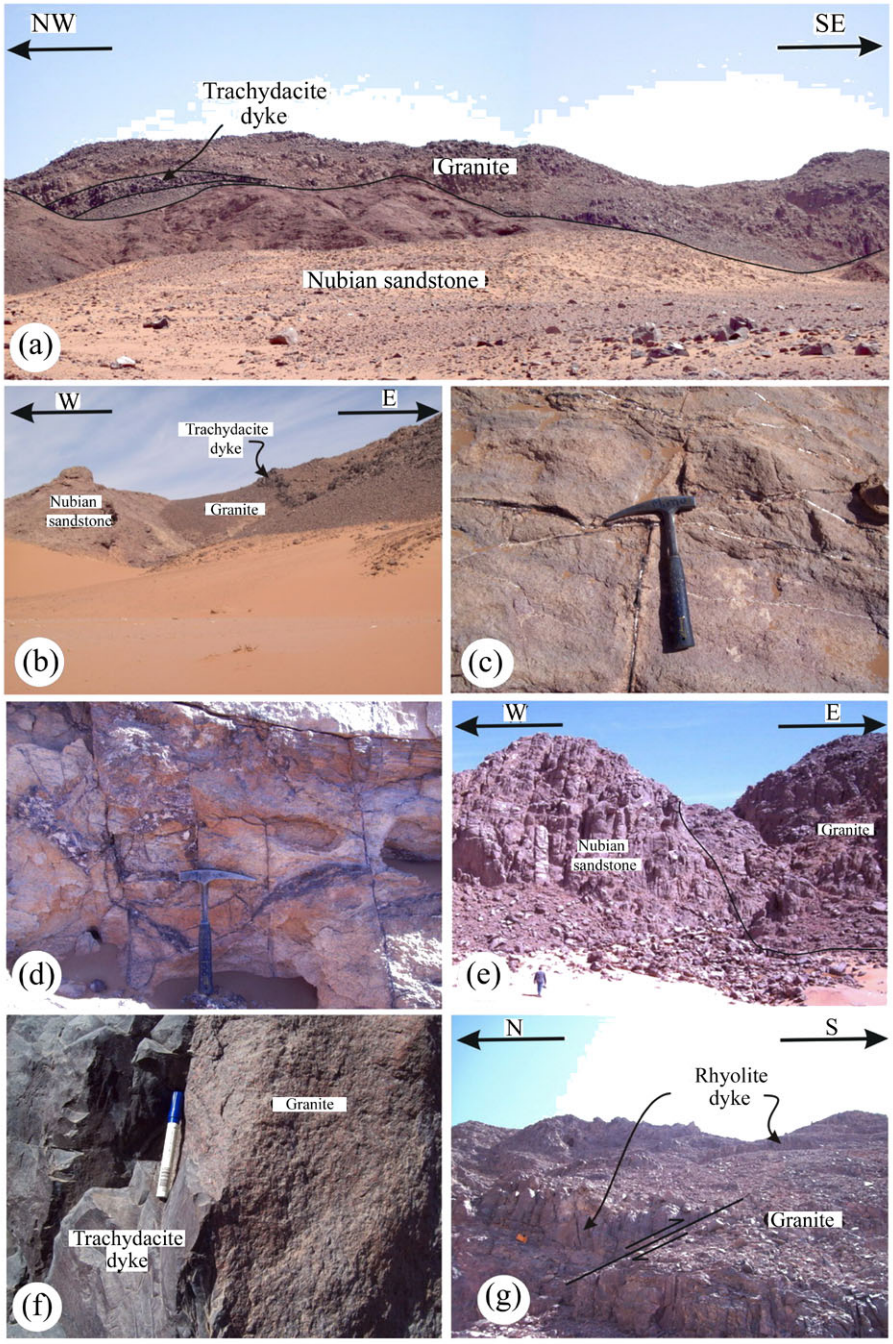

Fig. 2. Photographs showing (a) panorama view of the granite cut by trachydacite dykes against the Nubian sandstones, (b) sharp contact between Nubian sandstones and granites, (c) quartzitic Nubian sandstones along contacts with granites, (d) alteration of Nubian sandstones and fracture filling with Mn-Fe oxides, (e) subvertical and inclined bedding of Nubian sandstones near the contact with granites, (f) sharp contact between trachydacite dyke and granites, (g) rhyolite dyke cut granites and dissected by dextral fault.

Table 1 Classification of the alkaline rocks in the South Eastern Desert (after El-Ramly et al., 1971)

Alkaline rock			
Ring complex	Incomplete ring complex (crescent-shaped intrusion)	Lava and the associated agglomerate plug (dome) and ring dyke	Isometric mass of alkaline granite and syenite
1. G. Abu Khruq 2. G. El Gezira 3. G. Mishbeh 4. G. Mansouri 5. G. Tarbtie	1. G. Zargat Naam 2. G. Nigrub El Tahtani	1. Basalt 2. Volcanic plug and extrusive dome 3. Ring dyke	1. G. Shabeh 2. G. Maladob 3. G. Silaia 4. Stock-like body of Wadi Natash

The western contacts between the granitic mass and the Nubian sandstones are nearly vertical (Fig. 2e), inclined to bed with the dip angles around 60°−70° due to reactivation of NW-SE fault movements. At a distance of about 200 m from the contact, the sandstone beds of the Nubian sandstone are nearly horizontal.

The granitic mass as a whole is cut by a series of thick sub-latitudinal dykes composed of trachydacite (2−3 m in width) and rhyolite (0.5−1.5 m in width). They are exposed in the center to western parts of the main mass. These dykes have crescent shapes and extend northwestwards dipping steeply towards the centre of the granitic mass (60°−80°). The trachydacite and rhyolite dykes cut the granites with distinct sharp contacts (Fig. 2f). The trachydacite dykes are relatively more frequent than the rhyolite dykes and usually dissected by NE-SW dextral fault (Fig. 2g).

Relics of small trachybasalt lava flows are encountered in the northeastern part of the mapped area. These lavas lie without contact with granites and the outcrops ranges from 300 to 600 m. These rocks are represented by two flows trending NW-SE (Fig. 1) and extend eastward to the outside of the study area. They may be related to the Natash volcanic rocks (trachybasalt, trachyandesite and trachytes) (Ibrahim, 2010).

3 Petrography

The studied granites are medium- to coarse-grained yellowish pink in color and mainly composed of potash feldspars, quartz, plagioclases and aegirine-augite. Zircon, apatite, allanite and opaques are accessories. Sericite, kaolinite and epidote are secondary minerals. Potash feldspars (66.4 vol.%−70.5 vol.%) are represented by the orthoclase perthites and perthites, characterized by patchy and string types. The orthoclase perthite forms anhedral to subhedral crystals up to 4 mm in length and shows simple twinning.

Quartz (22.1 vol.%−24.3 vol.%) is fine- to medium-grained crystals up to 2.5 mm across and sometimes show undulose extinction. They are intergrown with feldspars forming skeletal shape and graphic textures (Fig. 4a). This intergrown feldspar represents a later generation corresponding to the simultaneous crystallization of feldspar and quartz interstitial. Plagioclases ($An_{8–14}$) are less common (1.2 vol.%−3.6 vol.%) and mainly represented by albite. Some antiperthite plagioclase crystals grow along with the perthite peripheries and sometimes corroded by quartz.

Aegirine-augite crystals (2.1 vol.%−4.6 vol.%) show green color and are pleochroic from yellowish green to green (Fig. 4b). They are represented by euhedral to subhedral crystals (up to 0.6×2.5 mm) having various outlines which occur between quartz and alkali feldspars. Some aegirine-augite crystals are altered to dark green chlorite associated with deep red iron oxides arranged along the cleavage planes of mafic minerals (Fig. 4c).

Xenotime occurs as rounded shaped crystals either as inclusions or interstitial between crystals (Fig. 4d). Zircon is also associated with opaques (Fig. 4e) either as inclusions or interstitial between crystals. Apatite occurs as fine prisms interfiling between crystals (Fig. 4f). Allanite forms eubhedral dark brown crystals (Fig. 4g) and are often coated with yellow-brown alteration products likely limonite (Klein and Dutrow, 2007). Opaques occur as fine irregular grains associated aegirine-augite crystals.

The data of modal analyses of the studied granitic samples (Table 2) fall in the alkali-feldspar granite field of the QAP diagram (Streckeisen, 1976) (Fig. 3).

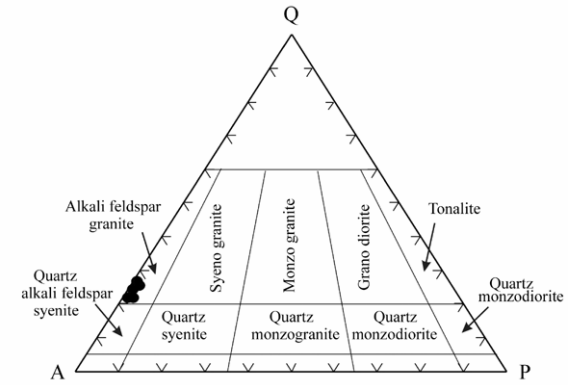

Fig. 3. QAP modal classification diagram of granitoids (Streckeisen, 1976).

The trachydacite dykes are fine-grained, massive, reddish brown to grayish brown in color and exhibit aphanitic and porphyritic textures (Fig. 4h). They are essentially composed of plagioclases, potash feldspars, quartz and biotite. Epidote and opaques are the main accessories. Plagioclases ($An_{25–28}$) occur as subhedral tabular oligoclase phenocrysts up to 6 mm in size and as minute laths (0.2×0.4 mm) forming the groundmass with quartz. Potash feldspars are usually perthite tabular phenocrysts up to 4 mm in size. Quartz occurs as anhedral interstitial grains (0.1×0.3 mm), forming the main components of the groundmass with plagioclase. Biotite is presented as yellowish brown flaky crystals. Epidote and opaques are usually associated the mafic.

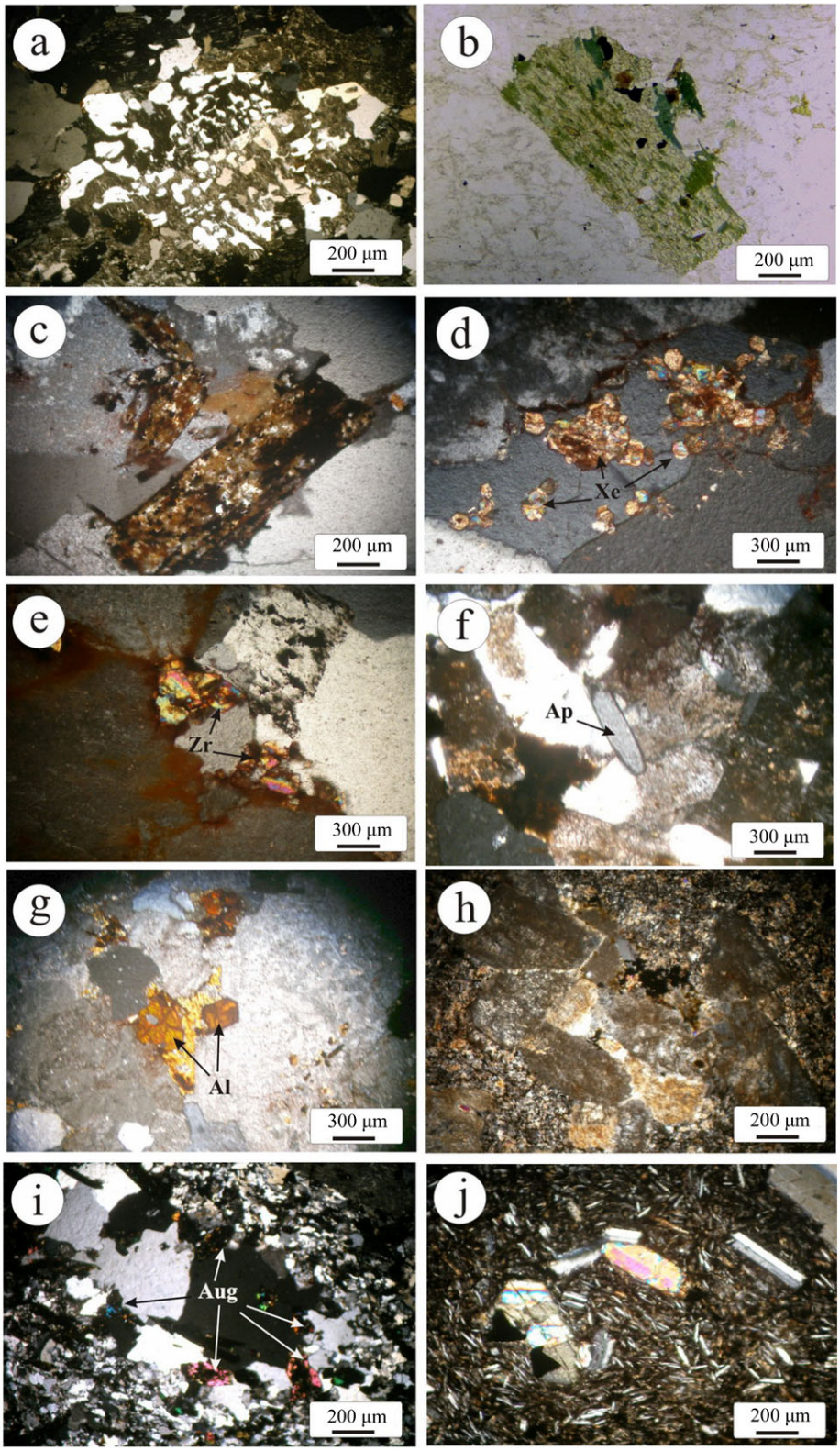

Fig. 4. Photomicrographs showing graphic texture in granite (a), aegirine-augite under plane polarized in granites (b), altered aegirine-augite to dark green chlorite with releasing deep red iron oxides in granites (c), aggregates of rounded xenotime (Xe) in granite (d), zircon (Zr) associated with opaques in granites (e), apatite (Ap) in granite (f), euhedral allanite (Al) in granite (g), porphyritic texture in trachydacite dyke (h), porphyry quartz and euhedral augite (Aug) in rhyolite dyke (i), trachytic and porphyritic textures in trachybasalt flow (j).

Table 2 Modal analysis for the studied granites, East Gabal Nuqra

S. No.	K-feld	Plag	Qz	Aeg-aug	Op	Acc	A	P	Q
1	70.5	1.6	21.4	4.6	2.3	0.6	75.4	1.7	22.9
2	69.7	1.4	22.6	3.9	2	0.5	74.4	1.5	24.1
3	70.1	1.2	22.1	3.7	2.5	0.4	75.1	1.3	23.6
4	69.1	3.6	22.5	2.1	2.1	0.6	72.6	3.8	23.6
5	68.5	2.1	24.1	2.6	2.2	0.5	72.3	2.2	25.5
6	67.4	2.1	24.3	3.4	2.4	0.4	71.9	2.3	25.8

Note: S. No. serial number; K-feld. potash feldspar including perthite; Plag. plagioclase; Qz. quartz; Aeg-aug. aegirine-augite; Op. opaques; Acc. accessories; A. potash feldspar content; P. plagioclase content; Q. quartz content. All values are in volume percent.

The rhyolite dykes are fine-grained with massive appearance having pale reddish brown colors and aphanitic to porphyritic textures (Fig. 4i). They are mainly composed of quartz, potash feldspars, plagioclases, augite and biotite. Zircon, apatite, allanite and opaques are accessories. Quartz shows weak wavy extinction and poikilitically enclosed in perthites. Potash feldspars are represented by orthoclase perthite phenocrysts (up to 5 mm in size) of the string type, as well as anhedral fine crystals in the groundmass. Plagioclases occur as fine crystals in groundmass of equant shape. Augite occurs as euhedral to subhedral crystals (Fig. 4j). It is pleochroic from yellow to green and brown in colors with Z^c=20º−24º. Biotite is less common and forms subhedral to euhedral small flakes.

The trachybasalt flows are fine-grained, greenish-black in color and mainly composed of plagioclase, alkali feldspar (sanidine) and augite while opaques and apatite are accessories. The plagioclases, augite and pseudomorphic chlorite phenocrysts embedded in fine plagioclase laths, forming porphyritic and trachytic textures (Fig. 4j).

4 Mineralogy and radioactivity

The accessory minerals (Fig. 6) have been investigated by scanning electron microscope (ESEM) supported by energy dispersive spectrometer (EDS) unit and X-ray diffraction (XRD) techniques at the Nuclear Materials Authority of Egypt. The samples were crushed and the size fraction between 0.063−0.5 mm was used. This size fraction was subjected to systematic mineral separation techniques using heavy liquids (Bromoform, 2.8 sp. gr.), magnetic fractionation using Frantz Isodynamic Magnetic Separator and microscopically handpicking mineral grains.

Xenotime (YPO_4) is yttrium phosphate mineral. It occurs as pale yellow rounded crystals interfiling between crystal boundaries or as inclusions. The crystals show weak pleochroism and cracked as a result of radioactive constituents. The heavy rare earths (dysprosium, erbium, terbium and ytterbium) and metal elements (thorium and uranium) replace yttriums which are considered as secondary components of xenotime (Fig. 6a).

Zircon ($ZrSiO_4$) occurs as euhedral to subhedral crystals, having colorless, yellow or pale brown colors. It forms in silicate melts enriched with incompatible elements and incorporate them into its structure. The substituting elements commonly present are Y, REEs, Hf, Th and U replacing Zr (Speer, 1980) (Fig. 6b).

Apatite occur as pale grey of elongated crystals interfiling between crystal boundaries or as inclusions. It is identified by XRD as fluor-apatite [$Ca_5(PO_4)_3F$]. It contains significant amount of rare earth elements and Th (Fig. 6c).

Allanite occurs as euhedral to subhedral deep brown crystals, showing pleochroism from pale brown to dark brown. It has the general formula $A_2M_3Si_3O_{12}[OH]$ where the A sites can contain large cations such as Ca^{2+} and Sr^{2+}, and light rare earth elements, and the M sites admits Al^{3+}, Fe^{3+}, Mn^{3+}, Fe^{2+}, or Mg^{2+} among others. However, a large amount of additional elements, including Th, U, Zr, P, Ba, and Cr, contains up to 20% rare earth elements being a valuable source of them (Dollase, 1971) (Fig. 6d).

Uranium and thorium anomalies have been detected from radiometric maps of Aero Service Division, Western Geophysical Company of America (1984) (Fig. 5). The distribution of natural gamma radioactivity in the various rock types has been measured in the field (using portable GR-512).

Table 3 shows that, the average eU and eTh contents increase gradually from the dykes to granitic rocks while the anomalous spots along fractures and faults show high average values (16×10^{-6} eU and 52×10^{-6} eTh) especially those enriched with ferrugination. Mostafa et al. (2010) identified some minerals from the anomalous spot including REE-silicate mineral, Pb-carbonate, kasolite and barite. They considered it controlled by faults and fractures (trending 25°N −77°W) that act as the pass way for hydrothermal solutions.

It can be concluded that, the presence of high radioactivity in the granites is controlled lithologically and structurally. This can be attributed to the tendency of U and Th due to their large ionic radii and charge to

concentrate in the residual magma indicating that, the enrichment is due to magmatic processes. These features coincide with the presence of xenotime, zircon, apatite and allanite accessory minerals which acted as the source of Y, U, Th and REEs.

Table 3 eU ($\times10^{-6}$), eTh ($\times10^{-6}$) and eTh/eU ratio of different rock types, East Gabal Nuqra

Rock type		eU ($\times10^{-6}$)	eTh ($\times10^{-6}$)	eTh/eU
Trchybasalt flow (*n*=6)	Min.	0.5	1	2
	Max.	2	3	1.5
	Average	0.8	2	2.5
Rhyolite (*n*=14)	Min.	3	8	2.7
	Max.	10	21	2.1
	Average	5	11	2.2
Trachydacite (*n*=16)	Min.	2	5	2.5
	Max.	8	18	2.3
	Average	4	9	2.3
Granite (*n*=38)	Min.	4	9	2.3
	Max.	14	26	1.8
	Average	8	16	2
Anomalous spot along fracture in granite (*n*=18)	Min.	8	14	1.8
	Max.	40	94	2.4
	Average	16	52	3.3

Note: *n*=number of measurements.

5 Geochemistry

Fifteen samples from the study area (3 trachydacites, 3 rhyolites and 9 granites samples) were analysed using wet chemical techniques (Shapiro and Brannock, 1962) for major oxides (wt%) and XRF technique for trace elements ($\times10^{-6}$). The data are listed in Table 4. All the chemical analyses were carried out at the Nuclear Materials Authority (NMA) of Egypt. Analytical accuracy of the data was found to be better than ±3% for major oxides and within ±5%–±10% for trace elements. Eight samples from the examined rocks (4 granite, 2 trachydacite and 2 rhyolite samples) were analyzed in the Atomic Energy Labs of Egypt for rare-earth elements (REEs). The accuracy of the results was found to be in the range 5%–10% for the rare earth elements.

5.1 Major, trace and rare-earth elements

5.1.1 Major and trace elements

The classification and nomenclature of the studied granites and associated dykes are carried out using Cox et al. (1979) TAS (total Alkali Silica) diagram for plutonic rocks classification, while the dividing line between alkalic and sub-alkalic magma series is from Irvine and Baragar (1971). The granite samples are plotted in the alkali granite field except one sample in the subalkaline field (Fig. 7a). The TAS for volcanic rocks after Le Bas et al. (1986) is used to classify the studied dykes which are plotted in the trachydacite and rhyolite fields (Fig. 7b).

The studied granites are characterized by high contents of SiO_2 (72%), total alkalies (9.6%), Rb (177×10^{-6}) and high field strength elements (HFSE) such as Zr (1529×10^{-6}), Nb (100×10^{-6}) and Y (624×10^{-6}) and low contents of MgO, CaO, Ba and Sr which are typically similar to A-type granites.

Based on the Alumina saturation diagram of Maniar and Piccoli (1989), the diagram shows that the investigated granites and rhyolite samples mainly show alkaline affinity, while the trachydacite samples indicate metaluminous affinity (Fig. 7c).

Batchelor and Bowden (1985) proposed a diagram of R_1-R_2 of De la Roche et al. (1980) to discriminate the different tectonic settings of the granitoid rocks. The granite samples fall between alkaline to sub-alkaline trends and are emplaced during anorogenic stage (Fig. 7d).

Fig. 8 of Whalen et al. (1987) shows the examined granitic samples plot in the A-type granite field. The variation diagrams ($Ga/Al\times10^4$ vs. K_2O+Na_2O, K_2O+Na_2O/CaO, K_2O/MgO, and FeO^T/MgO ratios), of Fig. 8a, b, c and d show that the studied granites plots in the A-type granites field. Also the variation diagrams of HFSE (Zr, Y, Nb and Zn vs. $Ga/Al\times10^4$) (Fig. 8e, f, g, and h) show that the granites plots in the A-type granites field.

The SiO_2-Al_2O_3 binary relation of Maniar and Piccolli (1989) shows that, the examined granite samples plot is mainly in the field of continental epeirogenic uplift granite (CEUG) and rift related granites (RRG) (Fig. 7e). The Rb vs. Y+Nb and Nb vs. Y discrimination diagrams of Pearce et al. (1984) (Figs. 7f and g) show that the studied granite samples is plotted in within-plate granite field (WPG).

The trachydacite and rhyolite samples are entirely related to within-plate magma field, using Nb-SiO_2 diagram (Fig. 7h) after Gass (1979). Twist and Harmer (1987) reported that, the high-Mg felsites (dacite-rhyolite) emplaced related to the volcanic arc while the low-Mg felsites (trachydacite-rhyolite) are similar in composition to the granites and granophyre suites and emplaced in within-plate tectonic setting and related to the A-type.

5.1.2 Rare-earth elements (REEs)

In order to investigate the relative content and the fractionation trends of the REEs in the studied rocks, their contents and averages are normalized to chondritic values after Anders and Grevesse (1989) (Table 5).

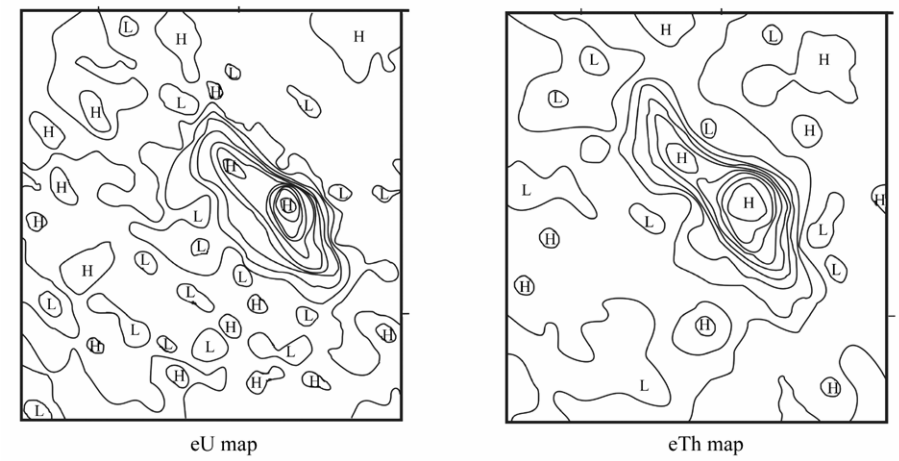

Fig. 5. eU and eTh distribution maps of the studied area, after Aero Service Division, Western Geophysical Company of America (1984).

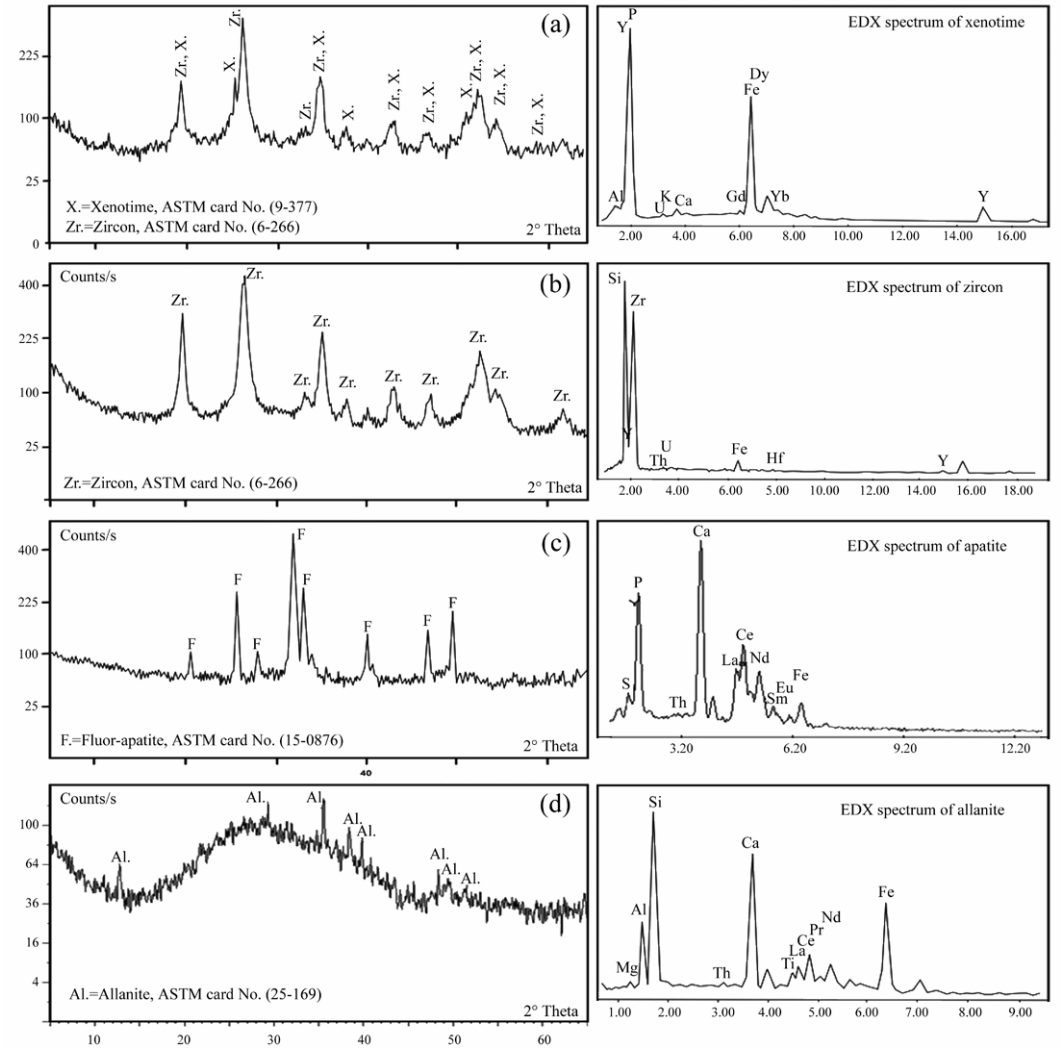

Fig. 6. XRD-patterns and EDX spectrum of xenotime, zircon, fluor-apatite, allanite and granite samples.

Table 4 Major oxides and trace-element analyses of the studied granites and associated dykes, East Gabal Nuqra

	Granite										Trachydacite dyke				Rhyolite dyke			
	S-1	S-2	S-3	S-4	S-5	S-6	S-7	S-8	S-9	Av.	S-10	S-11	S-12	Av.	S-13	S-14	S-15	Av.
SiO_2	72.83	72.28	72.01	71.32	71.88	71.66	72.11	72.4	72.09	72.06	61.23	62.11	61.64	61.66	72.11	71.48	71.88	71.82
TiO_2	0.49	0.42	0.41	0.19	0.4	0.17	0.39	0.13	0.18	0.31	1.18	1.21	1.16	1.18	0.49	0.38	0.46	0.44
Al_2O_3	12.51	12.56	12.67	12.5	12.31	12.32	12.11	12.11	12.18	12.36	15.3	15.22	15.12	15.21	11.55	11.35	11.65	11.52
Fe_2O_3	1.15	1.32	1.83	2.72	2.38	2.71	1.38	2.15	2.21	1.98	3.25	3.28	3.29	3.27	1.11	1.41	1.32	1.28
FeO	0.89	1.1	0.84	0.61	1.16	0.71	1.5	0.54	0.69	0.89	2.68	2.38	2.46	2.51	0.84	1.11	0.98	0.98
MnO	0.03	0.03	0.04	0.04	0.05	0.02	0.08	0.03	0.04	0.04	0.07	0.08	0.07	0.07	0.04	0.04	0.05	0.04
MgO	0.32	0.19	0.28	0.38	0.14	0.51	0.45	0.69	0.75	0.41	2.51	2.54	2.56	2.54	0.28	0.39	0.36	0.34
CaO	0.98	0.89	0.93	1.28	1.15	1.27	1.21	1.32	1.13	1.13	3.18	3.11	3.21	3.17	0.93	1.41	1.11	1.15
Na_2O	4.41	4.32	4.28	4.91	4.15	4.13	3.92	4.9	4.85	4.43	5.44	5.38	5.41	5.41	5.21	5.15	5.26	5.21
K_2O	5.32	5.21	5.11	5.12	5.22	5.31	4.89	5.02	5.11	5.15	4.32	4.24	4.42	4.33	6.13	6.15	6.02	6.1
P_2O_5	0.41	0.38	0.29	0.33	0.26	0.22	0.28	0.12	0.15	0.27	0.15	0.14	0.16	0.15	0.29	0.23	0.22	0.25
L.O.I.	0.52	0.65	0.48	0.51	0.54	0.53	0.72	0.52	0.55	0.56	0.71	0.62	0.61	0.65	0.87	0.89	0.87	0.88
Total	99.86	99.35	99.17	99.91	99.64	99.56	99.04	99.93	99.93	99.60	100.02	100.31	100.11	100.15	99.85	99.99	100.18	100.01
Ba	279	295	216	400	286	230	389	277	390	307	311	304	298	304	244	250	242	245
Rb	218	229	132	183	179	145	132	181	194	177	110	96	101	102	215	211	187	204
Sr	67	96	25	28	44	35	18	36	26	42	456	230	658	448	108	117	113	113
Zr	2567	3706	993	337	1679	1371	690	1404	1017	1529	102	125	136	121	1218	1187	1089	1165
Nb	131	153	84	58	121	93	64	112	81	100	31	34	28	31	46	52	44	47
Y	1091	1128	443	167	763	622	304	638	459	624	71	88	79	79	649	101	466	405
V	3	4	51	9	8	4	6	5	6	11	1	2	2	2	8	6	4	6
Ga	22	19	23	20	22	18	19	18	21	20	20	21	18	20	18	19	16	18
Cr	62	51	50	40	52	43	50	45	36	48	26	32	30	29	50	41	38	43
Ni	10	10	5	7	6	8	8	7	7	8	4	6	5	5	8	7	6	7
Cu	6	5	9	9	9	9	9	8	9	8	19	17	18	18	6	8	7	7
Zn	119	127	156	74	131	71	77	135	71	107	22	38	32	31	107	87	88	94
Pb	13	14	2	3	8	2	3	5	6	6	29	10	19	19	18	16	15	16
Hf	141	220	87	38	86	67	46	77	56	91	18	18	23	20	66	54	44	55
Rb/Sr	3.3	2.4	5.3	6.5	4.1	4.1	7.3	5.0	7.5	5.1	0.2	0.4	0.2	0.3	2.0	1.8	1.7	1.8
Y/Nb	8.3	7.4	5.3	2.9	6.3	6.7	4.8	5.7	5.7	6.3	2.3	2.6	2.8	2.6	14.1	1.9	10.6	8.6

Table 5 REE ($\times 10^{-6}$) analysis of the studied granites and associated dykes (trachydacites and rhyolites), East Gabal Nuqra

	Granite					Trachydacite			Rhyolite		
	S-1	S-4	S-5	S-7	Av.	S-10	S-11	Av.	S-13	S-14	Av.
La	31.1	30.45	32.4	29.8	30.94	25.4	26.5	25.95	91.36	93.13	92.25
Ce	68.25	70.52	64.73	66.17	67.42	39.1	25.9	32.5	160.08	158.12	159.10
Pr	8.65	5.4	7.52	4.02	6.40	6.15	6.27	6.21	21.4	22.31	21.86
Nd	39.12	22.9	39.9	18.7	30.16	30.72	32.9	31.81	69.32	77.41	73.37
Sm	9.3	4.09	7.9	3.2	6.12	6.19	6.2	6.2	15.9	16.13	16.02
Eu	0.68	0.46	0.68	0.43	0.56	1.9	1.96	1.93	0.75	0.73	0.74
Gd	9.7	3.53	8.9	2.92	6.26	4.3	4.65	4.48	11.09	12.18	11.64
Tb	1.39	0.55	0.8	0.44	0.80	0.82	0.79	0.81	2.21	2.41	2.31
Dy	10.5	3.2	8.89	2.25	6.21	4.87	5.41	5.14	11.9	12.85	12.38
Ho	2.24	0.72	1.9	0.66	1.38	0.5	0.7	0.6	2.65	2.77	2.71
Er	6.75	2.11	5.9	1.9	4.17	2.61	2.8	2.71	6.75	6.91	6.83
Tm	1.1	0.29	0.89	0.3	0.65	0.34	0.4	0.37	1.26	1.35	1.31
Yb	7.92	1.89	6.41	1.79	4.50	1.61	1.7	1.66	6.8	6.59	6.70
Lu	1.06	0.27	0.79	0.2	0.58	0.26	0.25	0.26	0.92	0.95	0.94
∑LREE	156.42	133.36	152.45	121.89	141.0	107.56	97.77	102.7	358.1	367.1	362.6
∑HREE	40.66	12.56	34.48	10.46	24.54	15.31	16.7	16.01	43.58	46.01	44.8
∑REE	197.76	146.38	187.61	132.78	166.1	124.77	116.43	120.6	402.4	413.8	408.1
∑LREE/HREE	3.85	10.62	4.42	11.65	7.63	7.03	5.85	6.44	8.22	7.98	8.1
Eu/Eu*	0.22	0.36	0.25	0.42	0.31	1.06	1.06	1.06	0.16	0.15	0.16
$(La/Yb)_N$	2.72	11.15	3.5	11.53	7.23	10.92	10.79	10.86	9.3	9.87	9.54
$(Gd/Yb)_N$	1.01	1.54	1.15	1.35	1.26	2.21	2.26	2.23	1.35	1.53	1.44
$(La/Sm)_N$	2.1	4.67	2.57	5.84	3.79	2.57	2.68	2.63	3.6	3.62	3.61

Note: $_N$. normalized values after Anders & Grevesse (1989).

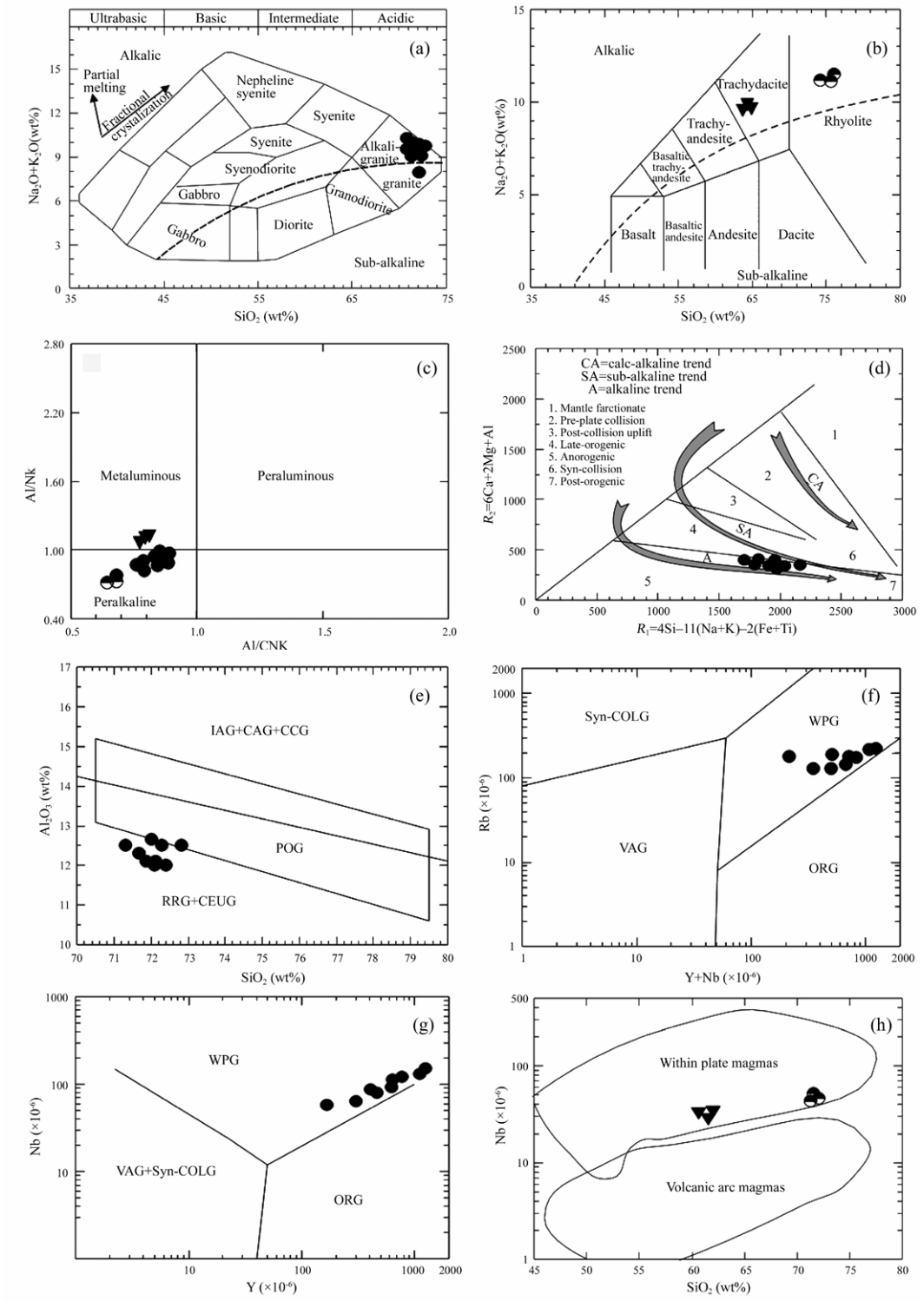

Fig. 7. (a) Nomenclature of plutonic rocks of Cox et al. (1979), the dividing line between alkalic and sub-alkalic magma series is from Irvine and Baragar (1971); (b) chemical classification of volcanic rocks using TAS (total alkali-silica diagram) after Le Bas et al. (1986); (c) $Al_2O_3/(Na_2O+K_2O)$ versus $Al_2O_3/(CaO+Na_2O+K_2O)$ diagram of Maniar and Piccoli (1989); (d) R_1–R_2 diagram of Batchelor and Bowden (1985); (e) Al_2O_3 versus SiO_2 diagram of Maniar and Piccoli (1989); (f) Rb versus Y+Nb diagram of Pearce et al. (1984); (g) Y versus Nb diagram of Pearce et al. (1984); and (h) Nb-SiO_2 discrimination diagram of Gass (1979).

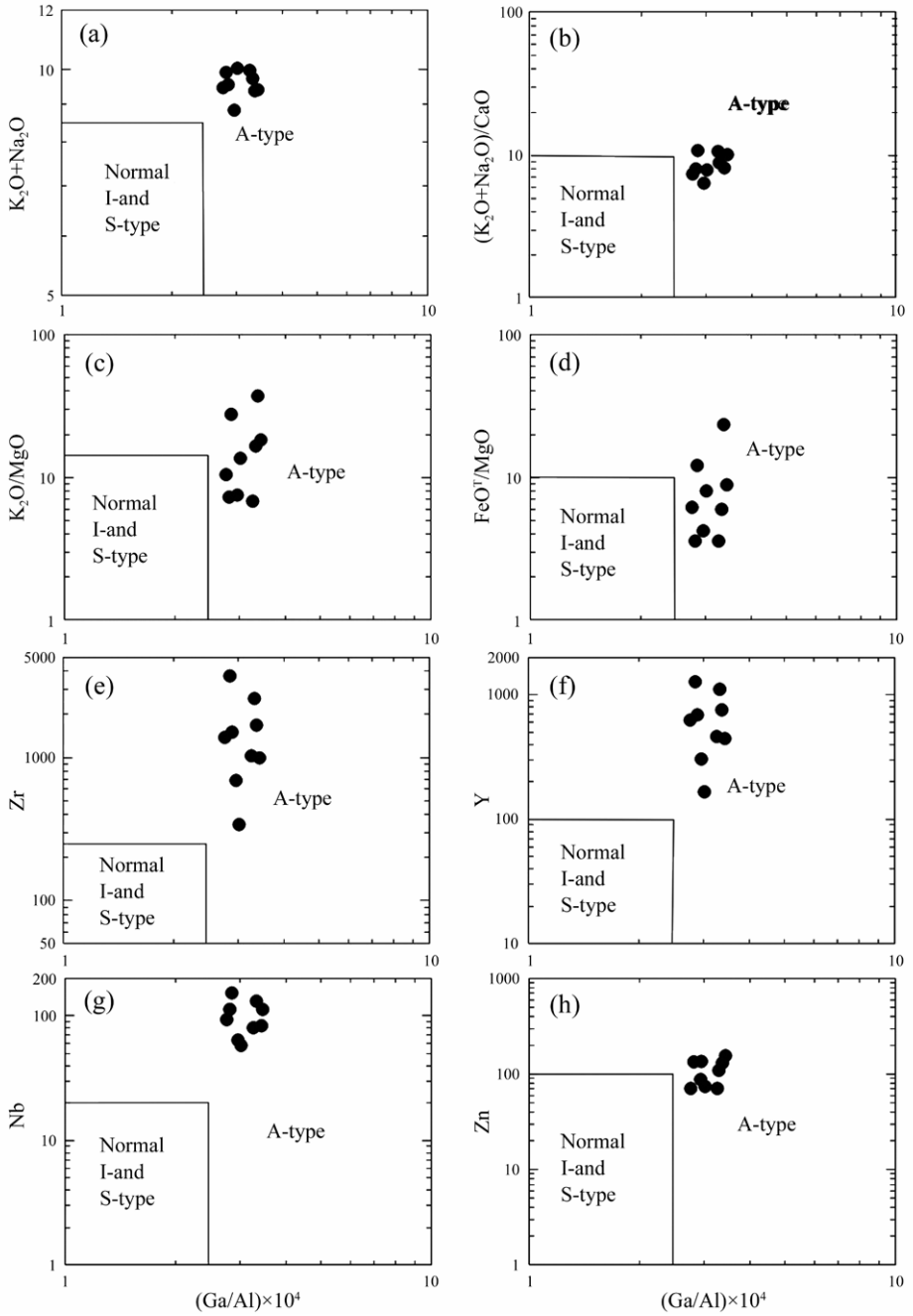

Fig. 8. Whalen et al. (1987) discrimination diagrams, (Ga/Al×10^4) against K_2O+Na_2O (a); K_2O+Na_2O/CaO (b); K_2O/MgO (c), FeO^T/MgO (d); Zr (e); Y (f); Nb (g); and Zn (h).

The average of the total REEs content of the studied granite ($\sum$REE=166×10^{-6}) is lower than that of the world-wide granite ($\sum$REE=250×10^{-6}–270×10^{-6}) as given by Hermann (1970). The depletion of REEs has been attributed to various processes including magmatic differentiation (Cuney and Friedrich, 1987), hydrothermal leaching (Cathelineau, 1987) and or a combination of both.

The four granite sample patterns (Fig. 9) show that, the two samples (S.1 and S.5) are more enriched in REE than the other two samples (S.4 and S.7). As a measure of the degree of fractionation of LREEs and HREEs, both $(La/Yb)_N$ and $(Gd/Yb)_N$ ratios were used. The REE pattern of the studied granites shows high REE fractionation $(La/Yb)_N$=2.72–11.53 with an average of 7.23 and semi-flat HREE $(Gd/Yb)_N$= 1.01–1.54 with an average of 1.26. The two samples (S.1 and S.5) display small LREE-enrichment with $(La/Yb)_N$=2.72 and 3.5 respectively while the patterns of two samples (S.4 and S.7) show LREE-enrichment with $(La/Yb)_N$=11.15 and 11.53 respectively. The semi-flat HREE pattern indicates the effect of both xenotime and zircon being more pronounced in samples S.1 and S.5.

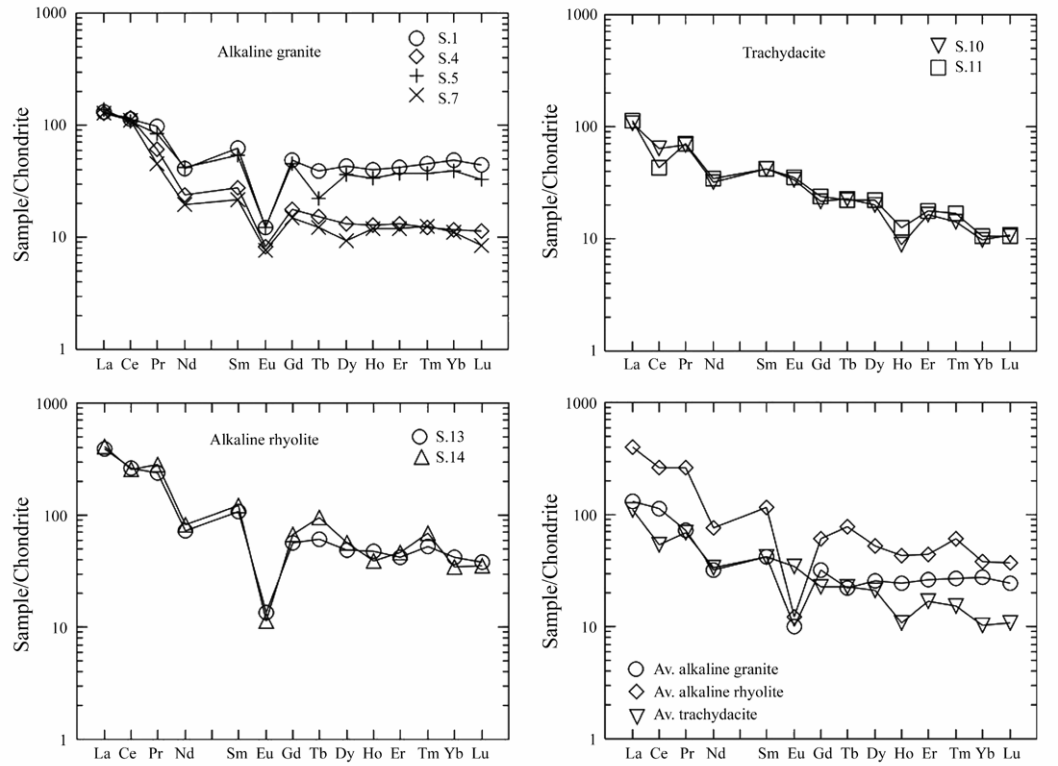

Fig. 9. Chondrite normalized REE patterns of the studied granites, trachydacite dykes and rhyolite dykes. Normalization is after Anders and Grevesse (1989).

The enrichment of LREE-content especially in S.4 and S.7 may be related to the presence of more allanite and apatite. The negative Eu anomalies displayed by the studied granites (Eu/Eu^*=0.22−0.42) are quite associated with their low Sr-contents (18×10^{-6}–96×10^{-6}), suggesting the removal of plagioclases during fractional crystallization (Neiva, 1992; Chappel et al., 1987).

The two trachydacite sample patterns (Fig. 9) show similarity in all REE values except Ce depletion in S.11 than in S.10 and Ho enrichment in S.11 than in S.10. The trachydacite display moderately fractionated REE pattern, sub-parallel and LREE enriched, where $(La/Yb)_N$=10.86. There is also a slight enrichment in the LREE where average $(La/Sm)_N$=2.63 and no-Eu anomaly where average Eu/Eu^*=1.06. These features as well as substantially higher Sr and lower transition metal abundances in plagioclase rich rocks are typical of intermediate magmas derived by small degree of partial melting of basaltic source regions in the upper mantle.

The two rhyolite sample patterns (Fig. 9) shows similarity in all REE values except Tb and Tm are slightly enriched in S.14 than in S.13. The fractionated trend patterns of rhyolite samples are characterized by $(La/Yb)_N$ ratio about 9.54. However, the rhyolite REEs patterns show more fractionated LREEs where the average of $(La/Sm)_N$=3.61 and semi-flat HREE pattern, $(Gd/Yb)_N$=1.44. The presence of a large negative Eu-anomaly in the rhyolites pattern reflects the removal of plagioclases during fractionate crystallization of an intermediate melt derived by partial melting from a basic source.

5.2 Petrogenesis

No single parent magma can produce all groups of alkaline rocks (Sorensen, 1974). They could originate through a number of processes, namely, (a) fractional crystallization from suitable parent magma, (b) low melting fraction of appropriate low silica parent magma, and (c) from sub-alkalic rocks by a process of desilication. Many alkaline suites represent fractionates of mantle-derived magma (Eby, 1990) characterized by having low Y/Nb ratio (<1.2), while other suites are characterized by higher Y/Nb ratios (1.2−7). This group shows a complex petrogenetic history, some suites have a significant mantle component whereas others may be totally of crustal origin. The studied granite is characterized by high Y/Nb ratios (Y/Nb=2.9−8.3 with av.=6.3) like alkaline suites designated as type-2 A-type granites (Eby, 1992).

The Rb/Sr ratio is used as a measure of magmatic differentiation increasing with higher degree of differentiation (Tsusue et al., 1988). Moreover, the higher Rb/Sr ratios (more than 1.5) suggest pre-existing fel-

sic material in the source region, while the Rb/Sr ratios of low value (less than 0.7) suggest derivation from the upper mantle. Accordingly, the examined granites with an average Rb/Sr ratio=5.1 suggests highly differentiated magma of crustal derivation.

6 Conclusions

The main mass of the East Gabal Nuqra is mainly alkali-feldspar granites cut by trachydacite and rhyolite dykes. Xenotime, zircon, apatite and allanite are accessories and acted as the source of Y, U, Th and REEs.

The studied granites of the East Gabal Nuqra are similar to type-2 A-type granites. They are characterized by high K_2O, Na_2O, Zn, Rb/Sr and Y/Nb ratios. The high field strength elements (HFSE) are enriched, especially Zr (1529×10^{-6}), Nb (100×10^{-6}), Hf (91×10^{-6}), Y (624×10^{-6}) and LREE (141×10^{-6}), whereas Ca, Mg, Sr and Eu contents are depleted.

The igneous rock types of the East Gabal Nuqra originated from metaluminous to peralkaline highly fractionated trachytic magma and were emplaced in the within-plate environment. This is consistent with the normalized REE patterns, where the fractionated REE-pattern of the trachydacites with no-Eu anomaly may represent the original source magma from which the granites and rhyolites were derived. The trachydacite is suggested to have been derived by small degree of partial melting (≤10%) of deep seated basic source.

The alkali-feldspar granites were derived from the trachydacite liquid by fractional crystallization (30%−50%) involving retention of plagioclases in residue, thus creating large Eu-anomalies. The alkali rhyolites were derived from the same liquid by more extensive fractional crystallization (>50%), creating more LREE fractionation and large Eu-anomaly.

The NW-SE right-lateral shear in the Upper Cretaceous (Meshref, 1990) caused extension of the area, causing the emplacement of the alkali-feldspar granites of the main mass along an incomplete ring faults (NW-SE trend) after that the trachydacite and rhyolite dykes were extruded as a result of cauldron subsidence due to continued extension.

Acknowledgements The authors are very grateful to Prof. Abdalla A. Abdel-Monem for the valuable suggestions, fruitful discussions and constructive review of the manuscript. The authors would like to express their special thanks for Prof. M.E. Ibrahim and Prof. F. Amar for the kind assistance and constructive discussions during this work.

References

Aero Service (1984) *Final Operational Report of Airborne Magnetic/Radiation Survey in Eastern Desert, Egypt* [Z]. Aero-Service Division, Western Geophysical Company, TX, USA.

Anders E. and Grevesse N. (1989) Abundances of the elements: Meteoritic and Solar [J]. *Geochim. et Cosmochim. Acta*. **53**, 197−214.

Batchelor R.A. and Bowden P. (1985) Petrogenetic interpretation of granitoid rock series using multicationic parameters [J]. *Chem. Geol*. **48**, 43−55.

Cathelineau M. (1987) U-Th rare earth elements mobility during albitization and quartz dissolution in granitoids: evidence from South East French Massif Central [J]. *Bull. Mineral.* **101**, 249−259.

Chappell B.W., White A.J.R., and Wyborn D. (1987) The importance of residual source material (restite) in granite petrogenesis [J]. *J. Petrol*. **28**, 1111−1138.

Cox K.G., Bell J.D., and Pankhurst R.J. (1979) *The Interpretation of Igneous Rocks* [M]. pp.450. Allen and Unwin, London.

Cuney M. and Friedrich M. (1987) Physicochemical and crystal-chemical controls on accessory mineral paragenesis in granitoids: Implications for uranium metallogenesis [J]. *Bull. Mineral.* **110**, 235–247.

De la Roche H., Leterrier J., Grandclaude P., and Marchal M. (1980) A classification of volcanic and plutonic rocks using R_1-R_2 diagram and major element analyses; its relationships with current nomenclature [J]. *Chem. Geol*. **29**, 183−210.

Dollase W.A. (1971) Refinement of the crystal structure of epidote, allanite, and hancockite [J]. *Am. Mineral*. **56**, 447−464.

Eby G.N. (1990) The A-type granitoids: a review of their occurrence and chemical characteristics and speculations on their petrogenesis [J]. *Lithos*. **26**, 115−134.

Eby G.N. (1992) Chemical subdivision of the A-type granitoids: Petrogenetic and tectonic implications [J]. *Geology*. **20**, 641−644.

El-Ramly M.F., Budanov V.I., and Hussein A.A. (1971) The alkaline rocks of South Eastern Desert [J]. *Geol. Surv. Egypt*. **53**, 110.

Gass I.G. (1979) Evolution modal for the Pan-African crystalline basement [J]. *Bull. Inst. App. Geol. Bull.* **3**, 11–20.

Hashad A.H. and El Reedy M.W.M. (1979) Geochronology of the anorogenic alkalic rocks, South Eastern Desert, Egypt [J]. *Ann. Geol. Surv. Egypt*. **9**, 81–101.

Hermann A.G. (1970) Yttrium and lanthanides, In *Handbook of Geochemistry* (ed. Wedepohl K.H.) [M]. pp.39. 57-71-Bl to 39, 57-71-0-9. Springer-Verlag, Berlin.

Ibrahim M.E. (2010) Laterites-bearing REEs, Wadi Natash, Southeastern Desert, Egypt [J]. *J. of Rare Earths*. **28**, 471−476.

Irvine T.N. and Baragar W.R.A. (1971) A guide to the chemical classification of the common volcanic rocks [J]. *Can. J. Earth. Sci*. **8**, 523−548.

Klein C. and Dutrow B. (2007) *Manual of Mineral Science* [M]. pp.500. Wiley Publishers.

Le Bas M.J., Le Maitre R.W., Streckeisen A., and Zanettin B. (1986) A chemical classification of volcanic rocks based on the total alkali-silica diagram [J]. *J. of Petrology.* **27**, 745−750.

Maniar P.D. and Piccoli P.M. (1989) Tectonic discrimination of granitoids [J]. *Geol. Soc. Am. Bull*. **101**, 635−643.

Meshref W.M. (1990) Tectonic framework. In *The Geology of Egypt* (ed. Said R.). [M]. pp.113−155. Balkema, Rotterdam,

Miller C.F. and Mittlefehldt D.W. (1982) Depletion of light rare-earth ele-

ments in felsic magma [J]. *Geology*. **10**, 129−133.

Mostafa M.S., Ibrahim I.H., and Hassaan A.H. (2010) Tectonic framework of East Gabal Nuqra area, South Eastern Desert, Egypt [J]. *Al-Azhar Bulletin of Sci*. **21**, 19−43.

Neiva A.M.R. (1992) Geochemistry and evolution of Jales granitic system, Northern Portugal [J]. *Chem. Erde*. **52**, 225−241.

Pearce J.A., Harris N.B.W., and Tindle A. (1984) Trace element discrimination diagrams for the tectonic interpretation of granitic rocks [J]. *J. Petrol*. **25**, 956−983.

Shapiro L. and Brannock W.W. (1962) Rapid analysis of silicate, carbonate and phosphate rocks [J]. *U.S. Geol. Surv. Bull*. **1144**, 56.

Sorensen H. (1974) *The Alkaline Rocks* [M]. John Wiley, London.

Wright J.B. (1973) Continental drift, magmatic provinces and mantle plumes [J]. *Nature*. **244**, 565–567.

Speer J.A. (1980) Zircon, reviews in mineralogy (ed. Ribbe P.H.) [J]. *Mineral. Soc. Amer*. **5**, 67−112.

Streckeisen A. (1976) To each plutonic rock its proper name [J]. *Earth Sci. Rev.* **12**, 1−33.

Tsusue A., Mizuta T., Tamai T., and Ishihara S. (1988) Granitic rocks of Southwest Japan: Trace element evidence reading their differentiation; Ba, Rb and Sr relationships [J]. *Min. Geol*. **38**, 509−515.

Twist D. and Harmer R.E.J. (1987) Geochemistry of contrasting siliceous magmatic suites in the Bushveld Complex: Genetic aspects and implications for discrimination diagrams [J]. *J. Volcano. and Geoth. Res*. **32**, 83−98.

Whalen J.B., Currie K.L., and Chappel B.W. (1987) A-type granites: Geochemical characteristics, discrimination and petrogenesis [J]. *Contrib. Min. Petrol*. **95**, 407−419.